PAPER

Check for updates

Oxygen-tunable endothelialized microvascular chip to assess hypoxia–reperfusion in sickle cell disease

Samantha R. Schad, [iD] [a] Joan D. Beckman,[b] Wilbur A. Lam [iD] [cde] and David K. Wood [iD] *[a]

A better understanding of hypoxia reperfusion (H/R) injury is needed to gain deeper insight into the mechanisms driving sickle cell disease (SCD) pathophysiology. Existing *in vivo* and *in vitro* models have yet to fully explain H/R, which is typically associated with harmful inflammatory processes but has also been linked to a protective effect ameliorating subsequent severe vaso-occlusion. To address this need, we developed a novel microfluidic platform that includes three-dimensional endothelial-lined microchannels within an oxygen-tunable environment. These features enable simulation of H/R, red blood cell (RBC) sickling, and vaso-occlusion on-chip. The endothelial network cultured on-chip is physiologically relevant and expresses crucial microvascular features such as 3D lumen structure and expression of functional endothelial markers. We utilized this platform to perform an occlusion assay, evaluating the effects of hypoxic preconditioning on RBC-endothelial interactions contributing to occlusion. Our results demonstrate that both sustained mild hypoxia and cyclic hypoxia endothelial treatment reduce the likelihood of SCD occlusion on-chip. Specifically, average vaso-occlusion rates of 8.89% and 11.78% were observed among endothelialized devices preconditioned to cyclic and sustained hypoxia, respectively, compared to 57.93% and 55.05% for the control groups. Additionally, we leveraged RNA sequencing to identify differential regulation of specific genes contributing to this protective outcome. Of note, hypoxia preconditioning resulted in significant modulation of *CYBB*, *RELN*, and *SERPINA1*. These results offer a better understanding of the mechanistic changes affecting the endothelium during H/R and also offer potential targets for further exploration and therapeutic intervention in SCD.

[a] Department of Biomedical Engineering, University of Minnesota, 7-122 Nils Hasselmo Hall, 312 Church St SE, Minneapolis, MN 55455, USA. E-mail: dkwood@umn.edu
[b] Department of Medicine, Division of Hematology, Oncology, and Transplantation, University of Minnesota, Minneapolis, MN, USA
[c] Wallace H. Coulter Department of Biomedical Engineering, Georgia Institute of Technology and Emory University, Atlanta, GA, USA
[d] Department of Pediatrics, Division of Pediatric Hematology/Oncology, Emory University School of Medicine, Atlanta, GA, USA
[e] Aflac Cancer and Blood Disorders Center of Children's Healthcare of Atlanta, Atlanta, GA, USA

Introduction

Sickle cell disease (SCD) is an inherited autosomal recessive disorder caused by a mutation in the hemoglobin β gene, leading to hemoglobin polymerization, red blood cell (RBC) sickling, and a cascade of pathophysiological events culminating in painful vaso-occlusive crisis (VOC).[1,2] Despite its discovery over a century ago, treatment options for the millions of people with SCD worldwide remain limited, highlighting the need for a better understanding of its underlying mechanisms.[3–5] Recently, increased attention has been paid to hypoxia reperfusion (H/R) injury as a driving mechanism of SCD pathology.[6–9] In SCD, H/R injury starts with an initial vaso-occlusive event leading to tissue hypoxia and/or ischemia. Next, reperfusion of this tissue by oxygenation generates a cascade of signaling events cumulating in a significant pro-inflammatory response. While H/R is classically thought to induce harmful inflammatory responses, mild or cyclic episodes of hypoxia may provoke a conditioning effect that protects against severe subsequent H/R injury.[7,10] Previous attempts to identify mechanisms that initiate this pro-survival phenotype are incomplete and contradictory.[6,7,10,11] Although some studies have begun to examine the effect of H/R preconditioning on various organs and tissue compartments,[12–14] the effect on the microvasculature itself is largely unexplored. A better understanding of how H/R generates cytoprotective preconditioning of the endothelium will inform our overall understanding of SCD pathophysiology and offer insight towards therapeutic intervention, and microfluidic models are aptly suited to address these questions.

Microfluidic models have become an important tool in the study of SCD due to their optical accessibility, cost effectiveness, and ease of integration with human cells.[15] In particular, the use of endothelialized microfluidics have been well documented as a means of investigating endothelial contribution to disease.[16–25] For example, Tsai *et al.* presented an endothelialized microfluidic platform in 2012 that simulated thrombosis and microvascular occlusion in various hematologic diseases.[20] Additionally, a number of groups have utilized acellular devices in the study of microvascular occlusion.[26–29] Man *et al.* introduced the OcclusionChip in 2020 which presented a new microfluidic platform for the investigation of RBC deformability and occlusion index, ultimately correlating hypoxia treatment with higher occlusion index in SCD.[27] Separately, our group has pioneered hypoxia-tunable microfluidics for the study of RBC rheology in SCD.[30–34] In particular, Szafraniec *et al.* utilized this platform to characterize the differential roles of viscosity and friction in sickle cell blood flow,[33] while Hansen *et al.* investigated the effects of several therapies on blood rheology and oxygen saturation.[30,31] Overall, these studies show the ability of physiologic models to more accurately investigate underlying mechanisms of hematologic disease. Endothelialized microfluidics, occlusion chips, and oxygen-tunable devices each offer distinct advantages in the study of SCD. However, no model exists that combines each of these key biological components to effectively study H/R in SCD.

Here, we report the development of a microfluidic platform that comprises three-dimensional endothelial-lined microchannels in an oxygen-tunable environment, thus enabling simulation of H/R under conditions relevant to the microvasculature. We used this microfluidic platform to investigate the likelihood of SCD donor blood sample occlusion on-chip and also to explore hypoxia-induced endothelial gene modulation. Our results offer a better understanding of the mechanistic changes affecting the endothelium during H/R and also support the hypothesis that H/R may offer a protective effect against vaso-occlusion in SCD.

Methods

Microfluidic device design and fabrication

The multi-layer microfluidic platform consists of (1) a gas reservoir to regulate oxygen tension in the device, initiating hypoxia and/or red cell sickling, (2) a hydration layer to prevent cell dehydration, and (3) a fully endothelialized cell layer to mimic a network of microvascular channels (Fig. 1).
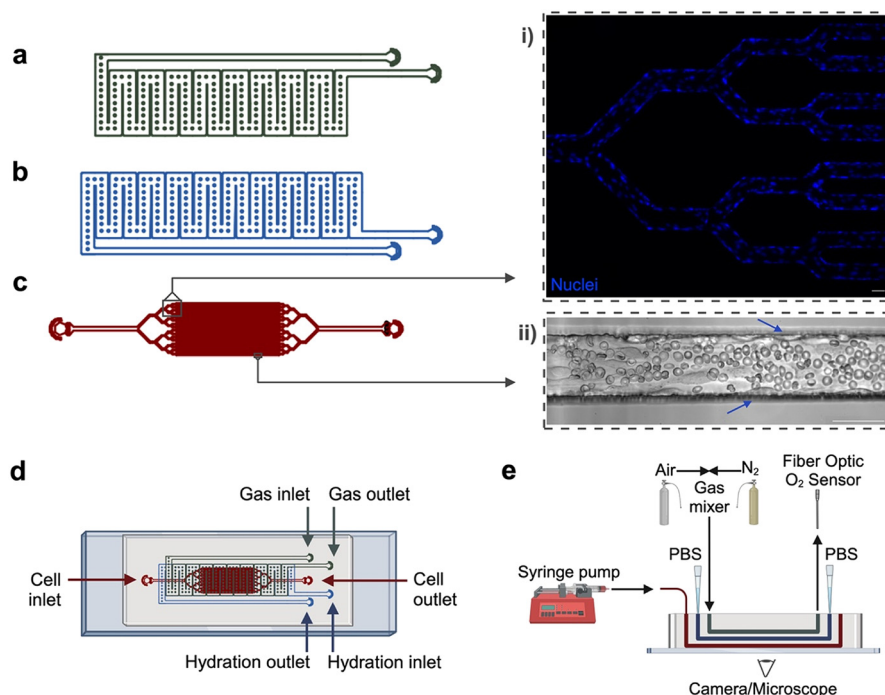

Fig. 1 Microfluidic device design and experimental setup. The microfluidic device is composed of three layers: (a) a gas reservoir to deliver oxygen, which initiates hypoxia and/or RBC sickling, (b) a hydration layer that prevents cell dehydration, and (c) a cell layer which is fully endothelialized to mimic the native microvascular system. The cell layer includes a branching network of 32 individual channels that can be observed under the microscope. Cell layer insets highlight (i) branching region of endothelialized device, stained to show nuclei, (ii) experimental region perfused with RBCs from a SCD donor. Arrows indicate endothelial cells lining the microchannel walls. (d) The multi-layer microfluidic device is fabricated *via* standard soft photolithography and PDMS techniques. Inlet/outlet ports allow access for gas delivery, gas sensing (gas reservoir), phosphate buffered saline delivery (hydration layer), device endothelialization, blood perfusion, and staining (cell layer). (e) The experimental setup includes a gas mixing system to directly control partial pressure of oxygen entering device, a fiber optic oxygen sensor, as well as access for liquid delivery *via* syringe pump or pipette. Created using AutoCAD, Inkscape, and Biorender. All scale bars indicate 50 μm.

The gas and hydration layer geometries are modified from our previous work, in which hypoxia has been used to examine sickle cell rheological properties in microfluidics lacking endothelium.[30–34] These two layers consist of wide, serpentine channels that directly overlap the cell layer. Due to the gas-permeable nature of PDMS, oxygen concentration in the cell layer can be directly controlled via gas input in the gas layer. The diffusive properties of similar devices have been previously validated using COMSOL modeling.[32] The cell-layer geometry is inspired by the branching nature of similar vascular networks on-chip, which allow for observation of a large number of microchannels in parallel.[16,19–21,35,36] Our bifurcating branching network resolves into 32 individual channels, each measuring 60 × 50 μm.

The device comprises three polydimethylsiloxane (PDMS) layers, each designed in AutoCAD and fabricated from silicon wafer molds using standard photolithography and soft lithography techniques. Individual silicon wafers were fabricated using SU-8 negative photoresist (SU-82100, SU-83050, Kayaku Advanced Materials) at the Minnesota Nano Center. The gas layer was cast with PDMS (Sylgard 184, Dow Corning) to a thickness of approximately ~6 mm, whereas the hydration and cell layers were cast via PDMS compression molding as previously described,[32] creating a 100 μm PDMS membrane at the cell layer/hydration layer and hydration layer/gas layer interfaces. The layers were adhered to each other and affixed to a glass microscope slide via oxygen–plasma bonding. Each layer was plasma bonded at an oxygen flow rate of 100 cc per minute with 100 W power for either 60 seconds (PDMS to glass) or 120 seconds (PDMS to PDMS) (PE-50, PlasmaEtch).

Cell culture

Pooled donor human umbilical vein endothelial cells (HUVECs) were obtained from ATCC. HUVECs were maintained in a humidified incubator at 37 °C, 5% CO_2 and cultured with endothelial cell growth medium-2 (EGM-2) (Lonza) supplemented with antibiotic-antimycotic (Gibco). Preliminary experimentation was also performed with human lung microvascular endothelial cells (HMVEC-Ls), which were cultured with microvascular endothelial cell growth medium-2 (EGM-2 MV) (Lonza) and antibiotic-antimycotic under similar conditions (Fig. S1). Cells were verified to be mycoplasma contaminant-free via the LookOut Mycoplasma Detection Kit (Millipore Sigma) and were used between passages 3–7. All samples for RNA work were derived from a single vial of pooled ATCC HUVECs to reduce effect of genetic variation by different donor lots.

Microfluidic device endothelialization

Microfluidic devices were first sterilized via UV treatment for 30 minutes. Then, a solution of 50 μg mL^{-1} fibronectin from human plasma in phosphate buffer solution (PBS) was added to the microfluidic device's cell layer via pipetting. The devices were incubated with fibronectin for 60 minutes, then rinsed twice with Hanks Balanced Salt Solution (HBSS). HUVECs were grown in cell culture flasks to approximately 80% confluency, trypsinized, and resuspended at a concentration of 15 × 10^6 cells per mL in a solution of 8% dextran-EGM-2 media. The presence of dextran in the cell resuspension increases the loading viscosity, thus increasing contact time (and adhesion) between endothelial cells and the microfluidic channel walls.[19] Cell suspension was added via pipette tip, reseeding ~4–6 times to coat at least 75% of the microchannel walls. To encourage proper cell attachment and spreading, devices were incubated under static conditions for ~90 minutes, then media was introduced at a rate of 60 μL h^{-1} using a New Era Syringe Pump. Perfusion at 60 μL h^{-1} approximated a flow rate of 1.875 μL h^{-1} in each of the smallest 60 μm-wide channels, which corresponded to a wall shear stress of ~1 dyne per cm^2 for blood.[19] Endothelialized devices were cultured under these flow conditions for 48 hours to establish a confluent monolayer and to encourage cell alignment under physiologic shear.[37] Before experimentation, all devices were examined under a microscope to assess quality. Any devices with gaps in the endothelium or irregular cell morphology were discarded to ensure high quality and consistency from experiment to experiment. Approximately 20% of devices were tossed from each experimental setup to maintain quality control standards. To account for this, a multiple of 1.5 times the desired number of devices were fabricated and endothelialized during each experimental setup to ensure sufficient device yield.

Fluorescence staining and microscopy of endothelialized devices

Numerous fluorescent stains, probes, and antibodies were used to thoroughly characterize the endothelium, including Hoechst 33258 (Invitrogen), CellMask Deep Red (Invitrogen), CD31 conjugated monoclonal antibody (Bio-Rad), CD144 monoclonal antibody (Invitrogen), CD106 recombinant antibody (Invitrogen), Phalloidin CruzFluor 594 (Santa Cruz), and cell permeable DAF-2 DA (Santa Cruz). DAF-2DA staining was performed on live endothelial cells, whereas all other stains were performed on cells fixed with 4% paraformaldehyde (PFA). Endothelial confluency and alignment were visualized using the CellMask plasma membrane and Hoechst nuclear stains. Adhesion marker expression was verified using conjugated (CD31), primary (CD144 and CD106), and secondary antibodies (Alexa Fluor 555 and 647) which were prepared at 1:100–1:250 in blocking buffer and incubated in blocked endothelialized devices at 4 °C overnight. Phalloidin was used to label F-actin, and solution was made at 1:100 in blocking buffer and incubated in blocked endothelialized devices at 4 °C overnight. Nitric oxide production was visualized with the DAF-2 DA fluorescent probe. DAF-2 DA solution was prepared at a dilution of 1:250 in EGM-2 media and perfused via

syringe pump to live endothelialized devices at a rate of 60 µL per hour for 1 hour prior to imaging. Microscopy was performed on either a Zeiss Axio Observer widefield microscope or a Nikon AX R confocal microscope. The widefield scope was equipped with an incubation chamber that maintained the environmental temperature to 37 °C. Image processing was performed in Zen software (Zeiss), NIS Elements software (Nikon), and FIJI/ImageJ. Cell confluence was measured as the percent area of each microchannel fluorescently labeled with CellMask plasma membrane stain. Cell density was calculated as the number of Hoechst-stained nuclei per mm^2 within the microchannels.

Hypoxic preconditioning

Endothelial hypoxic preconditioning was achieved using a solenoid valve gas mixing system that has been previously described.[32,34] Briefly, the gas mixer added compressed air (21% O_2, 5% CO_2, balance N_2) to compressed nitrogen (0% O_2, 5% CO_2, balance N_2) in a solenoid valve-controlled mixing chamber to achieve a user-specified oxygen concentration between 0 and 21%. Then, the gas at the desired oxygen concentration was perfused into the microfluidic device gas layer. Throughout experimentation, oxygen gas tension was monitored via a calibrated fiber optic oxygen sensor (NeoFox-GT, Ocean Optics). To maintain cell viability and alignment under flow, hypoxic preconditioning was performed in a 37 °C environmental chamber under consistent 60 µL h^{-1} media flow.

Endothelialized devices were exposed, or "preconditioned", to one of the following treatments for 60 minutes: (1) atmospheric control: 21% oxygen, (2) physiologic control: 12% oxygen, (3) cyclic hypoxia: alternating 12% oxygen and 5% oxygen at 10-minute intervals, or (4) sustained hypoxia: 5% oxygen. While most laboratory experiments are conducted at normal environmental oxygen levels (21% or 160 mmHg), it is important to note that this oxygen level is much higher than that of vasculature and tissue in the body. At sea level, arterial blood oxygen tension is typically between 75 and 100 mmHg, whereas venous blood oxygen tension is typically between 30 and 40 mmHg.[38,39] Therefore, we also chose to include a "physiologic" control, which would precondition the endothelial cells to a 12% (~90 mmHg) normoxia level resembling in vivo conditions.[38,39] For the hypoxia conditions, 5% oxygen level and 10-minute cycling intervals were based on preliminary experiments. Below 5% oxygen and more frequent (1 to 5-minute) cycling intervals negatively impacted endothelial cell viability and morphology. This parameter space may be further explored in subsequent work. After exposure to one of the four preconditioning treatments, endothelialized devices were returned the incubator (37 °C, 5% CO_2) and cultured under media flow for 4 additional hours. This window of time allowed the endothelium to respond to the preconditioning treatment and was chosen based on previous

studies on delay of genomic response in endothelial cells.[11,40]

Blood sample collection and preparation

Blood samples from individuals with SCD (HbSS and HbSC) were collected in citrate-coated vacutainers from Massachusetts General Hospital (MGH), Children's Hospitals and Clinics of Minnesota, and the University of Minnesota Medical Center (UMN). All samples were collected and experiments were performed in accordance with the guidelines of Institutional Review Boards at the Massachusetts General Hospital, at the University of Minnesota, and Children's Hospital and Clinics of Minnesota under approved protocols 2006P000066 (MGH) and STUDY00003 (UMN and Children's). Informed consent (and assent, if minor) were obtained from all human participants of this study. Routine clinical measurements, including complete blood count and hemoglobin variant analysis were performed on the samples (Table S1). Prior to use, blood samples were stored at 4 °C for a minimum of 2 hours and a maximum of 3 days.

Prior to an experiment, the whole blood sample was fractionated in a centrifuge (400g, 5 minutes × 3 wash cycles). The plasma and buffy coat layers were removed and replaced with PBS without calcium or magnesium to generate washed RBCs. Washed RBCs were gently loaded into a syringe with attached 0.015″ inner diameter tubing (BD Intramedic) and mounted on a syringe pump (Harvard Apparatus). Washed RBCs were used in this experiment to isolate just the contribution of the endothelium and RBCs in vaso-occlusion, decoupling variability from platelets, leukocytes, etc. Samples were loaded into new syringes for each microfluidic trial to limit the effect of red cell packing.

Occlusion assay

After the 4-hour incubation window, a preconditioned microfluidic device was placed in the 37 °C temperature-controlled microscope chamber equipped with a gas mixing system in preparation for the occlusion assay. The device preparation involved: (1) oxygen mixing system calibration, (2) PBS injection into hydration layer, (3) delivery of 12% oxygen into gas layer via solenoid mixing system, and (4) oxygen tension validation via NeoFox oxygen sensor. Once complete, washed RBCs from a SCD donor were perfused through the endothelialized cell layer at a rate of 60 µL h^{-1} using a syringe pump (Harvard Apparatus). All microfluidic devices underwent 10 minutes of RBC perfusion at physiologic oxygen levels (12% O_2) followed by 10 minutes of perfusion under hypoxia (5% O_2). During the experiment, bright field microscopy was monitored at 5–10× by scanning for clot formation and occlusion in each of the 32 parallel microchannels. Microchannel occlusion was defined as complete blockage/stasis of flow and occlusion incidence was measured at 5-minute intervals, quantified as percentage of the 32 microchannels fully obstructed within each device.

Reproducibility was assessed by performing this assay with a single HbSS genotype SCD donor sample across 5 independently fabricated and endothelialized microfluidic devices.

RNA extraction from microfluidic devices

To decellularize microfluidic devices, the endothelial cell layer was washed with 100 μL of HBSS, briefly rinsed with trypsin, and then incubated with trypsin for a 3-minute period to detach endothelial cells from the microchannel walls. Cells were then flushed from the device using 5% serum EGM-2 directly into a collection tube followed by a 5-minute centrifugation at 200g. The cell pellet was then resuspended in 100 μL PBS and RNA extraction was performed using the Norgen Biotek Single Cell RNA Purification Kit according to the manufacturer's instructions. After extraction, RNA samples were stored at −80 °C.

RNA quality testing, sequencing, and data processing

Frozen RNA samples were shipped on dry ice to Genewiz (Azenta) for quality testing and next-generation sequencing. Quality control testing *via* NanoDrop 2000, Qubit fluorometer, and Agilent TapeStation technologies confirmed sufficient sample concentration and integrity for downstream processing (Table S2). RNA sequencing workflow included polyA selection-based mRNA enrichment, mRNA fragmentation, random priming, first- and second- strand cDNA synthesis, end repair, 5′-phosphorylation, dA-tailing, adaptor ligation, PCR enrichment, and sequencing. Illumina sequencing configuration HiSeq with 2 × 150 base pair (bp) read length was used.

Sequence reads were trimmed using Trimmomatic v.0.36 to remove possible adapter sequences or nucleotides with poor quality. Trimmed reads were aligned to *Homo sapiens* GRCh38 reference genome. FeatureCounts from the Subread package v.1.5.2 was used to calculate unique gene hit counts. Comparison of gene expression between sample groups was performed in which the Walk test was used to generate p-values and log$_2$ fold changes. For each comparison, genes with an absolute log$_2$ fold change > 1 and an adjusted p-value < 0.05 were considered differentially expressed genes (DEGs). Gene ontology (GO) analysis was performed using GeneSCF v.1.1-p2 software, which used the Gene Ontology Annotation (GOA) human database to cluster genes based on their biological processes, noting statistical significances.

Statistical analyses

ANOVA statistical testing was performed using GraphPad Prism version 10.3.1. Occlusion incidence significance results were determined *via* one-way or two-way ANOVA testing, where appropriate. Geisser–Greenhouse correction was used to account for lack of sphericity/unequal variability of differences as recommended. A Tukey test for multiple comparison analysis was performed at a confidence interval of 95%/alpha threshold of 0.05. For correlative analysis, Spearman testing was performed in GraphPad Prism software. Correlation significance was indicated *via* p-value, in which * $p < 0.05$ and ** $p < 0.01$. In multiple statistical analyses, subgroup analysis was also performed to evaluate any potential effect due to transfusion by removing the three donor data sets who had a recent history of transfusion therapy (donor ID numbers 2, 3, and 12).

Results & discussion

Development of an endothelialized, oxygen-tunable microfluidic model to study SCD

A multi-layer platform was constructed to both control oxygen tension and culture endothelial cells on the same device, combining multiple aspects of SCD pathophysiology that have not previously been combined on-chip (Fig. 1). These features enable simulation of blood flow through microvascular channels, hypoxia-induced RBC sickling and H/R, and observation of RBC vaso-occlusion on a single device. The first layer acts as a gas reservoir to regulate oxygen tension, facilitating initiation of hypoxia, induction of RBC sickling, and evaluation of H/R injury (Fig. 1a). The second layer provides humidity and prevents cell dehydration (Fig. 1b). The third layer consists of a perfusable, fully endothelialized network of channels to mimic a microvascular network (Fig. 1c). The branching vascular network resolves into 32 individual channels, which permits observation of a large number of microchannels in parallel, similar to other vessel-on-chip geometries.[16,19–21,36] The size-scale (60 by 50 μm in the experimental region) and microchannel geometries were designed to mimic postcapillary venules–low oxygen microvasculature that are often associated with cell sickling, adhesion, and vaso-occlusion in SCD.[19,41,42]

Due to the challenging nature of the branching vessel geometry and small size scales, established protocols[19] for device endothelialization were incapable of fully endothelializing this geometry's thin branching network without clogs or bare regions. We refined a protocol to generate a confluent, aligned microvasculature system that recapitulates small vessels *in vivo* (see Methods). In particular, key advancements included: (1) increasing HUVEC seeding density to 15×10^6 cells per mL from commonly used ranges of $0.5–2 \times 10^6$ cells per mL, (2) repeated, intermittent seedings *via* pipette tip instead of *via* syringe pump to improve cell contact time with microchannel walls, and (3) 90-minute incubation period before adding flow to allow cells to fully attach and spread throughout channels. This method is versatile; preliminary experiments also demonstrated successful culture of microvascular endothelial cells (HMVEC-Ls) in device microchannels (Fig. S1). Overall, our microfluidic device design and experimental setup effectively enables cell culture of 3D endothelial vessel-structures in an oxygen-tunable environment. (Fig. 1d and e). Additionally, the design supports perfusion of donor RBCs and the

investigation of RBC-endothelial cell interactions driving SCD adhesion and vaso-occlusion.

Endothelialized microfluidics replicate key biological features of microvasculature

Fluorescence microscopy was used to evaluate the endothelium, including visualization of the vascular network and also confirmation of key physiologic attributes (Fig. 2). It was critical that our model system exhibited confluency along the microchannel, presence of a perfusable lumen, and alignment in the direction of flow.[43] Confocal microscopy was utilized to verify that endothelial cells in our microfluidic device effectively coated the top, bottom, and side walls of each microchannel while supporting a central lumen (Fig. 2a). Observation of the endothelium in the Z-direction also effectively confirmed endothelial confluency as well as alignment under flow. Cell confluence and density were quantified after 24- and 48-hour incubation windows to more thoroughly characterize the endothelium (Fig. S2). Endothelial cell

confluence and density improved with longer incubation under flow; in particular, density increased from 878 ± 110 to 1067 ± 122 nuclei per mm^2 between 24 and 48 hours of incubation (Fig. S2b).

Beyond confluency, lumen structure, and alignment, it was critical that the vascular network within the microfluidic device displayed key functional characteristics. These include expression of adhesion molecules, the ability to synthesize essential biological factors, the development of an organized cytoskeleton, and the ability to tolerate fluctuations in oxygen. Fluorescence microscopy was used to characterize the endothelium and identify the presence of physiologically relevant components. Adhesion molecules such as platelet endothelial cell adhesion molecule-1 (PECAM-1/CD31) (Fig. 2c) and vascular endothelial cadherin (VE-cadherin/CD144) (Fig. 2d) are associated with formation and maintenance of tight junctions between endothelial cells. Resultantly, these adhesion molecules contribute to barrier function and help maintain vascular homeostasis.[44] Vascular cell adhesion molecule-1 (VCAM-1/CD106) (Fig. 2e) also
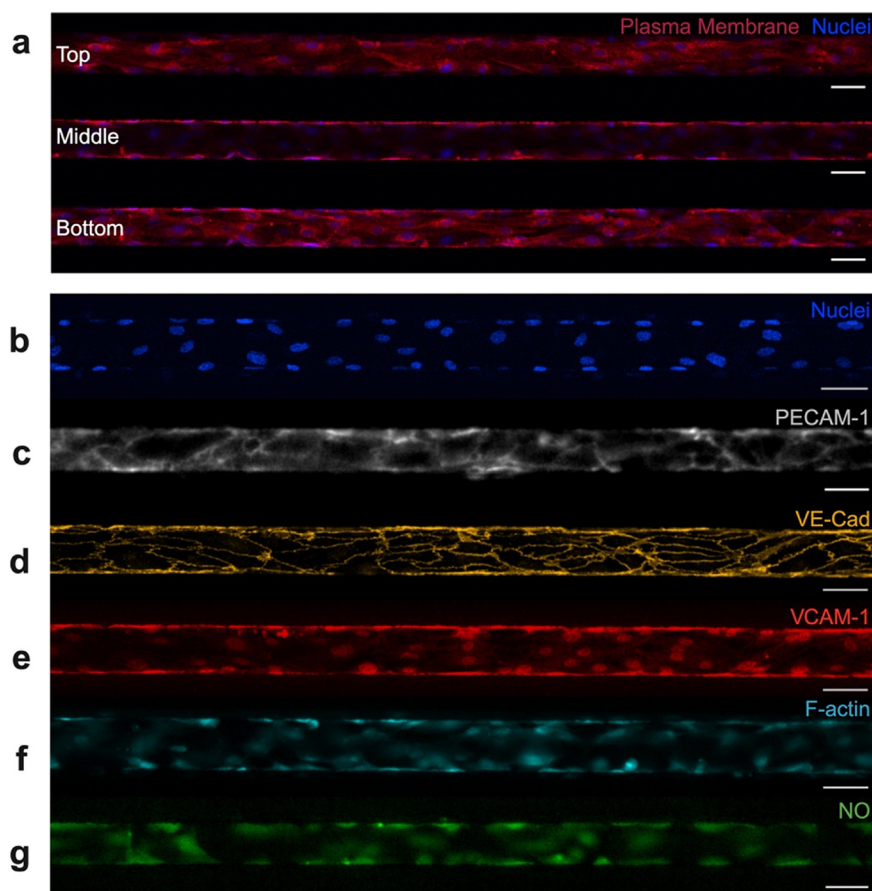

Fig. 2 Characterization of endothelium. Numerous fluorescent probes and techniques were used to visualize the endothelial cells and examine their physiologic relevance. (a) Confocal microscopy was used to verify 3D lumen structure and confluent microchannel lining. Top, middle, and bottom sections of the microchannel were fluorescently imaged after staining for nuclei (blue) and plasma membrane (red). HUVECs adequately cover the top, bottom, and side walls of the microchannel while maintaining a central lumen. Cells also align with flow in the horizontal direction. Fluorescent imaging of the device's experimental region highlights (b) confluency, via nuclear staining (blue), (c) PECAM-1 expression, (d) VE-cadherin expression, (e) VCAM-1 expression, (f) F-actin structures, and (g) nitric oxide production. All scale bars indicate 50 μm.

contributes to vessel wall integrity, while separately being shown to facilitate adhesion and recruitment of leukocytes to the endothelium.[44] PECAM-1, VE-cadherin, and VCAM-1 all play critical roles in endothelial function, and therefore it was necessary to confirm their presence in our endothelialized system. Each of these adhesion molecules have been successfully identified in our endothelialized microfluidics *via* fluorescent staining. To further validate the model, we confirmed the presence of filamentous actin (F-actin) *via* phalloidin staining (Fig. 2f). HUVECs normally express F-actin, a key component of the cytoskeleton. F-Actin contributes to endothelial structural support, cell barrier function, and cell–cell adhesion.[45,46] Lastly, we confirmed that HUVECs cultured in microfluidic devices

produce nitric oxide, another indicator of vascular function (Fig. 2g). Nitric oxide is synthesized by endothelial cells in the body, which is thought to modulate vascular homeostasis, vascular tone, and even protect blood vessels from injury.[47] Lastly, endothelialized devices underwent preliminary hypoxia testing, which validated that no loss of cells, detachment from microchannel walls, or significant morphological change occurred due to short-term hypoxia exposure (Fig. S3). Together, confirmation of adhesion molecule expression, cytoskeletal development, synthesis of biological factors, and tolerance to fluctuations in oxygen level demonstrate that the endothelium in our microfluidic devices morphologically and functionally resemble that of *in vivo* microvasculature.
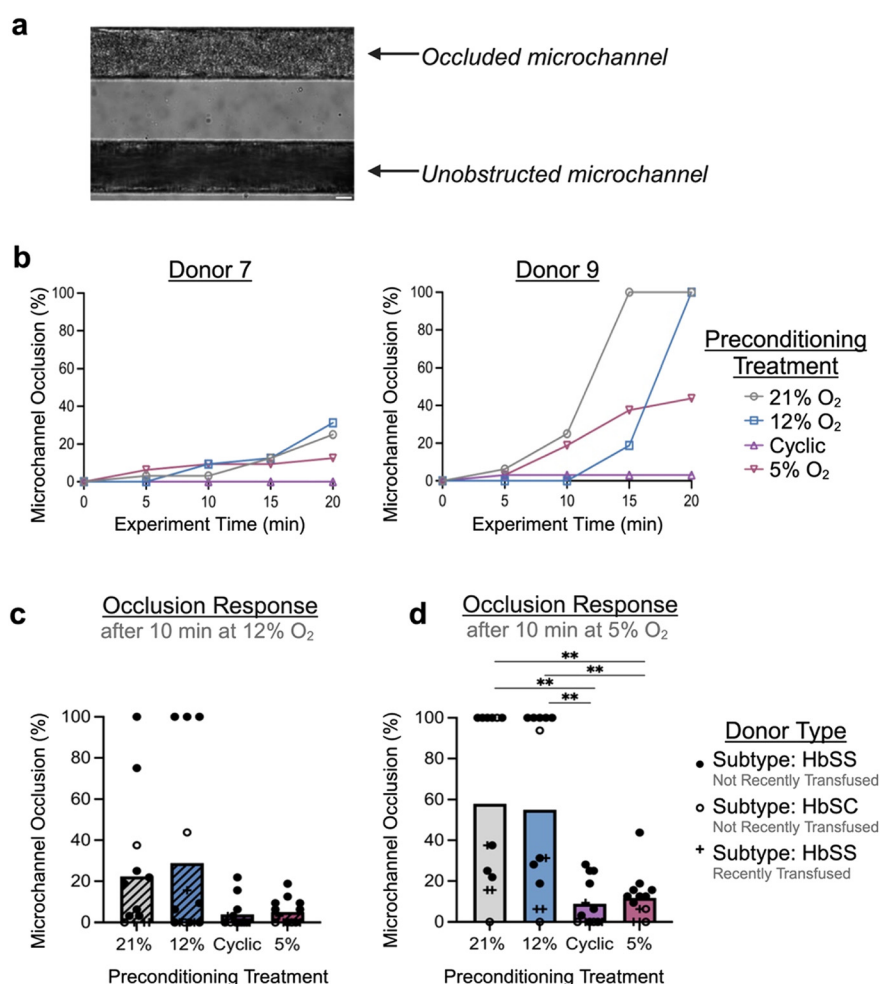

Fig. 3 Hypoxia preconditioning prevents vaso-occlusion. Blood occlusion assay can be used to track percentage of occluded microchannels over the course of an experiment. (a) Microfluidic device is optically accessible and allows for monitoring of occlusions as they develop on-chip. (b) Tracking of two representative samples that were perfused with RBCs from donors with SCD after devices were preconditioned to either atmospheric oxygen levels (21% oxygen), physiologic oxygen levels (12%), cyclic hypoxia (cycling of 12% and 5%), or sustained hypoxia (5%), as indicated by legend. Sample 9 had a considerably more occlusive response than sample 7 despite showing similar trends, indicative of donor-to-donor variability in the data set. (c and d) Incidence of microchannel occlusion in preconditioned devices was analyzed for all samples (c) after initial 10 minutes of RBC perfusion at 12% oxygen, a bimodal response began to emerge between preconditioning populations. (d) After subsequent 10 minutes of RBC perfusion at 5% oxygen, endothelialized devices preconditioned with either cyclic hypoxia or sustained hypoxia were protected from vaso-occlusion on-chip compared to both controls. Donor-specific information (genotype, transfusion history) is indicated by the legend. One-way ANOVA statistical testing was performed, *$p < 0.05$, **$p < 0.01$. Scale bar indicates 20 μm.

Hypoxic preconditioning reduces likelihood of SCD RBC microchannel occlusion

Other groups have recently pioneered the use of microfluidics to measure occlusion incidence on-chip as an indicator of clinical severity, a means of evaluating response to therapy, or as a tool for mechanistic study.[26,27,48,49] Our occlusive assay is unique in its functionality: incorporation of fully endothelialized microfluidic channels, ability to trigger H/R and hypoxia-mediated red cell sickling in real-time, as well as use of biologically relevant size scales/shear. Therefore, to test the effect of hypoxic preconditioning on likelihood of microchannel occlusion, RBCs from donors with SCD ($n = 13$) were perfused through endothelialized channels that had been preconditioned to one of four conditions: atmospheric control (21% O_2), physiologic control (12% O_2), cyclic hypoxia (cycling of 12% and 5% O_2), or mild sustained hypoxia (5% O_2). During an experiment, development of occlusive events was monitored in real-time (Fig. 3a), with percentage of device microchannel obstruction calculated each 5-minute interval (Fig. 3b; Fig. S4).

Across samples, compared to endothelialized devices conditioned at atmospheric or physiologic oxygen levels, devices preconditioned with either cyclic or sustained hypoxia exhibited a lower likelihood of microchannel occlusion. After the first phase of the experiment (during which the device was exposed to the physiologic level of 12% O_2), hypoxic preconditioned devices trended towards reduced microchannel occlusion (Fig. 3c). After the second phase of the experiment (during which the device was exposed to the hypoxic level of 5% O_2), devices preconditioned to hypoxia exhibited significantly lower microchannel occlusion compared to controls ($p < 0.01$) (Fig. 3d). Overall, we observed average microchannel occlusion rates of 8.89% and 11.78% after cyclic and sustained hypoxic preconditioning compared to 57.93% and 55.05% after atmospheric and physiologic controls, respectively. This result supports the hypothesis that mild or cyclic episodes of hypoxia can provoke a conditioning effect that protects against endothelial injury or vaso-occlusion. There was no significant difference between control conditions or, separately, between the two hypoxic conditions. As some donors had recently undergone transfusion therapy, we performed subgroup analysis excluding those donors which did not significantly affect the results or interpretation (Fig. S5). A reproducibility analysis was also performed by evaluating microchannel occlusion of a single SCD donor sample across five independently fabricated and endothelialized microfluidic devices, which indicated minimal chip-to-chip variability and a low coefficient of variation at later experimental timepoints (CV of 2.83% at the end of the experiment) (Fig. S6).

SCD donor clinical variables are correlated with microchannel occlusion on-chip

Phenotypic heterogeneity between SCD subjects with the same genotype is poorly understood.[1,50,51] Likewise, in our microvascular occlusion assay, there was notable inter-donor variation (Fig. S4). To further investigate this heterogeneity, we examined the correlation between occlusion outcomes and the donor clinical data set (Table S1). First, we performed a statistical analysis to determine if samples from either male ($n = 8$) or female ($n = 5$) donors were more likely to occlude. Based on our limited cohort, samples from male donors exhibited higher occlusion likelihood on-chip (Fig. S7). In the case of physiologic control, samples from male donors were significantly more likely to occlude than female donors ($p = 0.05$ for all samples, or $p < 0.05$ when excluding transfused samples). These results are consistent with the literature: In pediatrics, males exhibit higher pain crisis frequency than females (1.6 vs. 0.6 per year).[52] Moreso regardless of age, male SCD subjects experience more severe infectious and cardiovascular complications,[52] and overall worse SCD-associated morbidity and mortality rates.[53] Additional samples are needed to further validate this finding, but these initial conclusions prompt significant interest for future studies.

Next, we performed a nonparametric Spearman correlation to investigate the relationship between routine clinical measurements and percent occlusion in response to each type of hypoxic preconditioning treatment (Fig. 4; Fig. S8). Once again, statistical testing was conducted on all samples, then on non-transfused samples only. Across both analyses, a number of significant trends were observed. Hemoglobin and hematocrit demonstrated a weak inverse correlation with occlusion percentage across all groups but the atmospheric control. Generally, HbS, mean corpuscular volume (MCV), white blood cell count (WBC), and platelet count (PLT) exhibited moderate correlation with occlusion percentage across all groups. When analyzing the entire population sample set ($n = 13$), the results show significant correlation between sickle hemoglobin percentage (HbS) and percent occlusion in the 5% preconditioning group ($r = 0.769$, $p = 0.003$), between PLT and percent occlusion in the 5% preconditioning group ($r = 0.735$, $p = 0.006$), and between white WBC and percent occlusion in the 5% and 12% oxygen preconditioning groups ($r = 0.696$, $p = 0.01$, and $r = 0.612$, $p = 0.03$, respectively). When analyzing only non-transfused samples, we found a stronger correlation between both MCV and red cell distribution width (RDW) with occlusion, but a weaker trend between HbS and occlusion. In particular, a significant correlation was observed in the 5% preconditioning group between MCV and percent occlusion ($r = 0.714$, $p = 0.024$), between RDW and percent occlusion ($r = 0.689$, $p = 0.028$), and between WBC and percent occlusion ($r = 0.702$, $p = 0.085$). These results indicate that individuals with high levels of WBC, PLT, HbS, MCV, or RDW, as well as low levels of hemoglobin or hematocrit may exhibit a more occlusive, severe SCD phenotype. It was noted that the 5% preconditioning group exhibited a much stronger correlation with certain clinical parameters than other preconditioning groups. This finding may have been a result of the 5% preconditioning treatment more appropriately simulating the in vivo oxygen conditions. This result
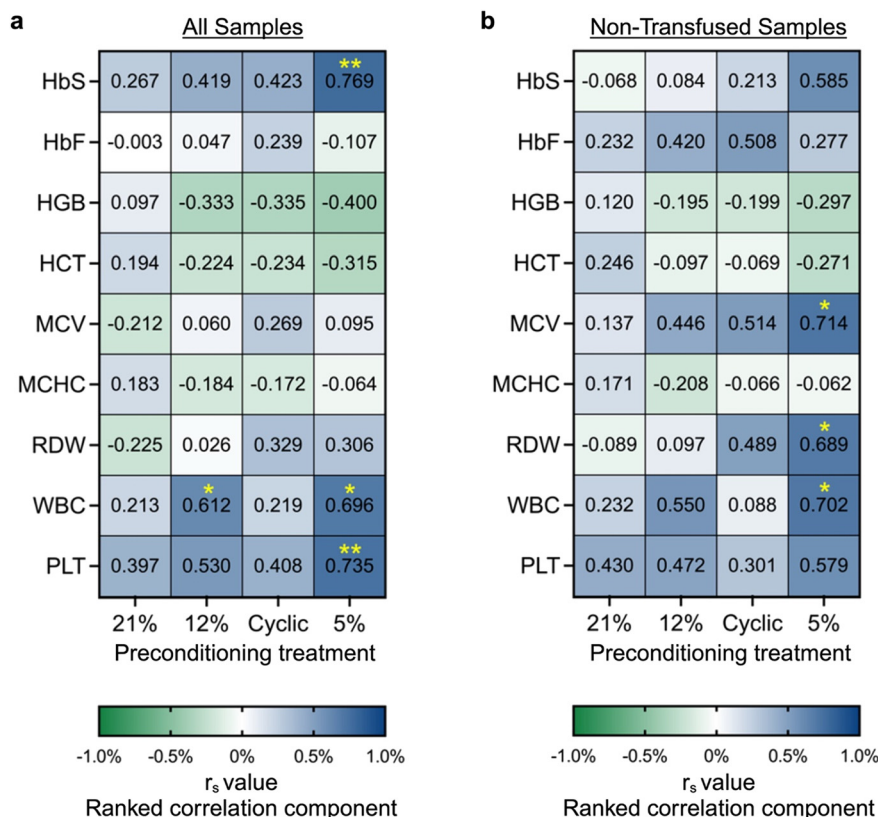
Fig. 4 Spearman correlation of routine clinical measurements with occlusion. A nonparametric spearman correlation was used to quantify correlation between routine clinical measurements and percent microchannel occlusion after various hypoxia preconditioning treatments. Spearman correlation r value was calculated for (a) all samples ($n = 13$) and (b) only non-transfused samples ($n = 10$). Clinical metrics were obtained from hemoglobin variant analysis and complete blood count testing, and consist of hemoglobin S (HbS), hemoglobin F (HbF), hemoglobin (HGB), hematocrit (HCT), mean corpuscular volume (MCV), mean corpuscular hemoglobin concentration (MCHC), RBC distribution width (RDW), white blood cell count (WBC), and platelet count (PLT). Ranked correlation component "r_s" ranges from −1 to 1 as indicated in the legend, with 0 indicating that the metrics do not vary together, 1 indicating perfect correlation, and −1 indicating perfect inverse correlation. Significance is indicated by asterisks, *$p < 0.05$, **$p < 0.01$.

highlights the importance of integrating physiologically similar environmental conditions and stimuli when developing biological models.

Evidence of a correlation between occlusion and non-RBC related indices (WBC and PLT) is particularly intriguing since the occlusion assay was performed using only RBCs. While others have shown that WBC and PLT counts are significantly elevated during VOC and high leukocyte counts have also been positively correlated with a number of SCD risk factors including early death, ACS, and stroke,[54] our study suggests that RBCs from SCD donors with leukocytosis and thrombocytosis exhibit higher occlusion capacity, even in hypoxia preconditioned endothelium. As leukocytosis and thrombosis may reflect systemic inflammation, further studies to assess how systemic inflammation in SCD may overcome the benefits of endothelial H/R preconditioning are warranted.

Hypoxic preconditioning causes transcriptional changes associated with vaso-occlusion

The ability of hypoxic preconditioning to prevent microvascular occlusion incidence in our devices led us to

investigate the hypoxia-induced gene-level changes to the endothelium. We developed a protocol to extract RNA from hypoxia-preconditioned endothelial cells cultured on-chip and then performed RNA-sequencing analysis (Fig. 5a). Despite the complexity of decellularizing the microfluidic devices, high cell viability was maintained which resulted in high quality and integrity RNA (Table S2). Compared to physiologic or atmospheric controls, both types of hypoxic preconditioning resulted in significant endothelial differential gene expression (Fig. 5b and c). Compared to sustained hypoxia, cyclic hypoxia resulted in more abundant differential gene modulation. We next performed gene ontology clustering to identify relevant enriched gene pathways modulated by hypoxic preconditioning (Fig. 5d; Tables S3–S6). We note significant modulation in critical pathways involving hypoxia sensitivity, blood vessel modification, coagulation, inflammation, adhesion, and endothelial cell functional behavior. Taken together, these changes in pathways of interest may contribute to the protective effect garnered by hypoxic preconditioning.

Next, we assessed volcano plots and heat maps (Fig. 6; Fig. S9), drawing attention to specific genes of interest. Cyclic
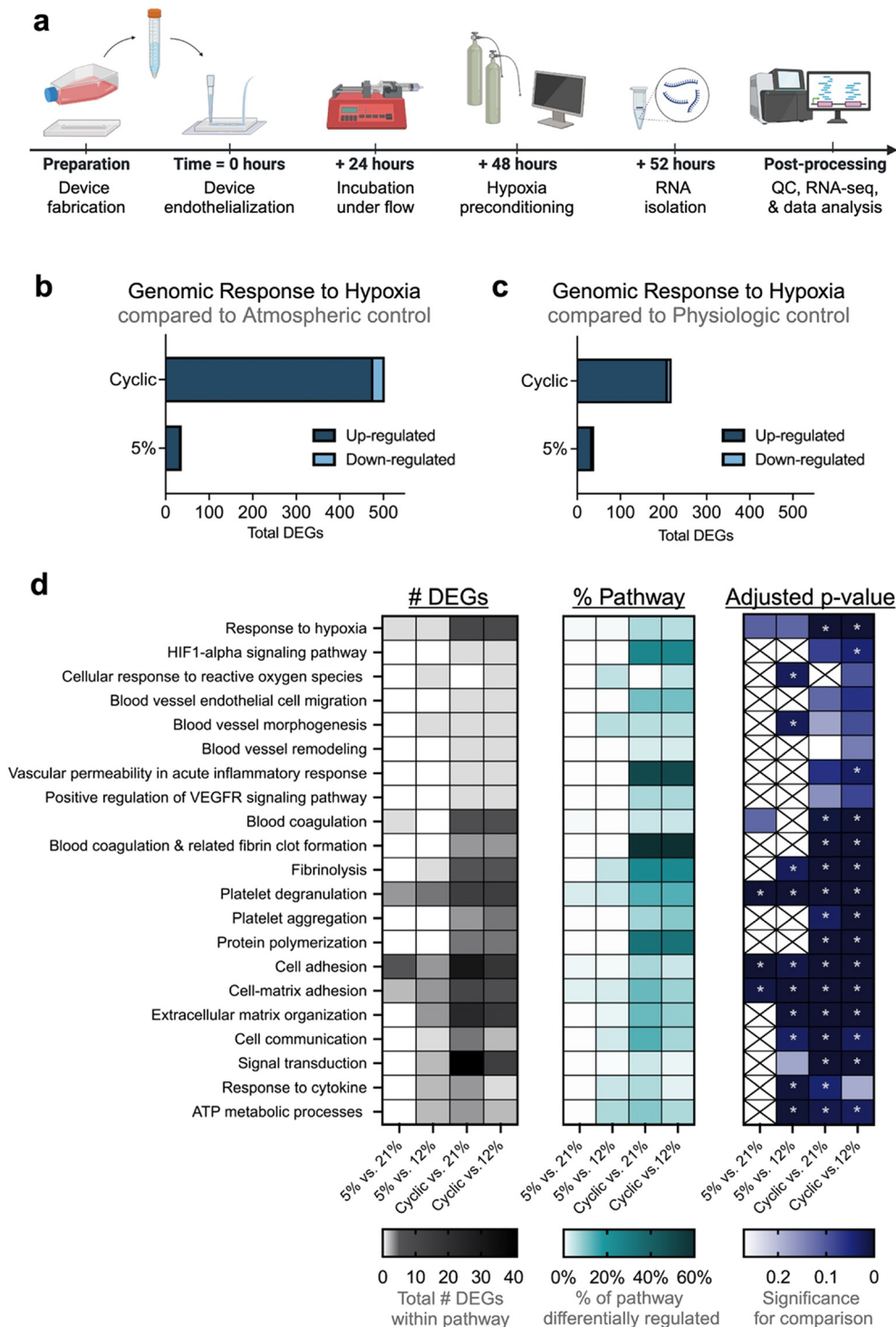
Fig. 5 RNA sequencing of hypoxia-preconditioned endothelium informs pathway analysis. (a) A methodology has been developed perform RNA sequencing on hypoxia-preconditioned endothelium from microfluidics. Microfluidic devices were seeded with human umbilical vein endothelial cells (HUVECs), cultured for 48 hours under flow, treated with various types of oxygen/hypoxia preconditioning, allowed to incubate for 4 additional hours, cells were then extracted from microfluidics for RNA isolation, and finally material was processed for RNA sequencing. (b and c) Effect of hypoxia preconditioning on endothelium cultured in microfluidic devices was examined in comparison to controls. (b) Compared to atmospheric control, cyclic hypoxia and sustained hypoxia preconditioning resulted in significant differential gene regulation of 503 genes and 37 genes, respectively. (c) Compared to physiologic control, cyclic hypoxia and sustained hypoxia preconditioning resulted in significant differential gene regulation of 219 and 39 genes, respectively. (d) For each comparison, differentially expressed genes were clustered by gene ontology using the Gene Ontology Annotation (GOA) human database for gene enrichment. Top relevant responses are included here, with more comprehensive data available in the supplement (Tables S3–S6). (Left panel) Number of differentially expressed genes in each ontology pathway are indicated by the gradient legend below the chart. (Middle panel) Percentage of differentially regulated genes in each pathway of interest are indicated by next legend. (Right panel) Adjusted p-value (also referred to as false discovery rate (FDR)) indicates confidence of each comparison. Data is significant when adjusted *p*-value < 0.05 *via* Fisher exact test, indicated by rightmost legend and denoted by asterisks. X's indicate lack of any DEGs in corresponding comparison.
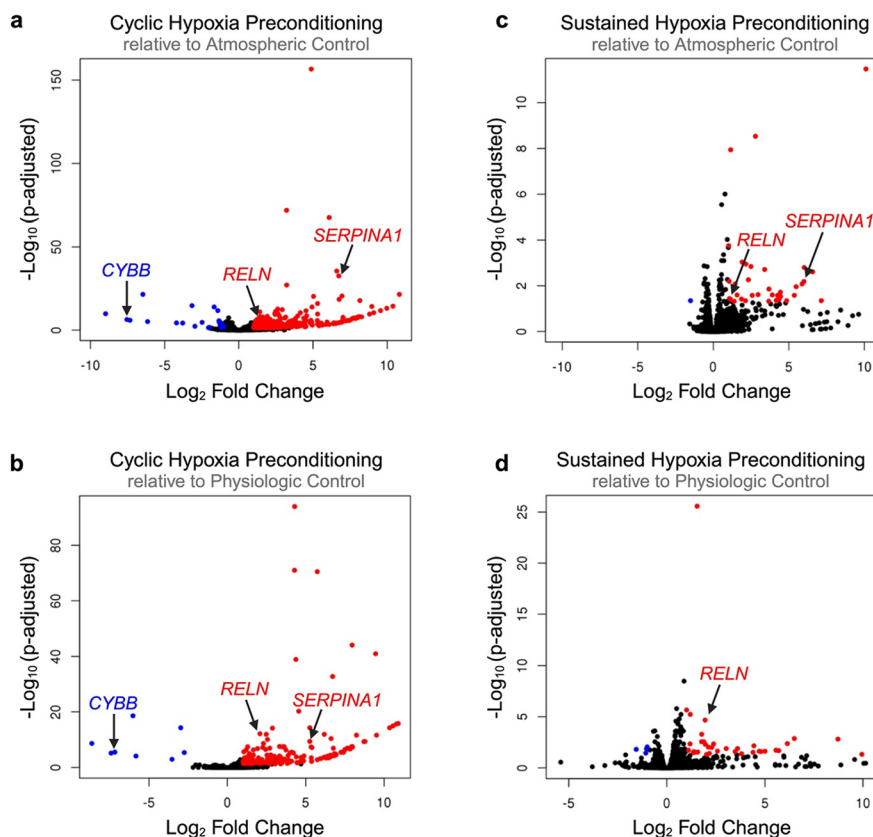
Fig. 6 Visualization of global transcriptional changes due to hypoxia preconditioning. RNA sequencing results are represented *via* volcano plots for each treatment comparison including (a) cyclic hypoxia preconditioning relative to atmospheric control, (b) cyclic hypoxia preconditioning relative to physiologic control, (c) sustained hypoxia preconditioning relative to atmospheric control, and (d) sustained hypoxia preconditioning relative to physiologic control. Upregulated genes (adjusted p-value < 0.05, $\log_2$ fold change > 1) are indicated by red dots. Down-regulated genes (adjusted p-value < 0.05, $\log_2$ fold change < -1) are indicated by blue dots. Significantly modulated genes of interest are marked with arrows.

hypoxic preconditioning resulted in a significant downregulation of the *CYBB* gene. The effect of cyclic hypoxic preconditioning nearly silenced *CYBB* expression, resulting in -7.55 and $-7.19 \log_2$ fold change in expression compared to atmospheric and physiologic controls, respectively ($p_{\text{adj}} < 0.001$ for both). The *CYBB* gene is included in the HIF1-α signaling pathway and encodes the cytochrome b-245 beta chain, a subunit of the NADPH oxidase protein (NOX2).[55] This is notable as NOX2 is known to be a major reactive oxygen species (ROS)-producing isoform. Our study suggests that exposure to cyclic hypoxia may suppress *CYBB*, which could result in cytoprotection through reduced NOX2-related ROS production.

Gene ontology and volcano plots also highlight the interaction between hypoxic preconditioning and numerous genes involved in coagulation and inflammation. In particular, *SERPINA1* was significantly upregulated in 3 of 4 comparisons (on average, a 6.00-fold change in differential gene expression, $p < 0.01$ for all 3 comparisons). The *SERPINA1* gene encodes the alpha 1-antitrypsin (AAT) protein, which inhibits inflammatory proteases.[56] Mutation in *SERPINA1* is correlated with venous thromboembolism and a number of pulmonary disorders.[57,58] AAT has also been shown to be elevated in SCD and positively correlated with

hemolytic and inflammatory patient indices, suggesting a relationship between AAT and disease severity.[56] Collectively, our data suggests that in SCD, endothelial H/R injury may drive AAT elevation and contribute to an overall pro-coagulatory, occlusive phenotype.

Additionally, a single adhesion-specific gene – *RELN*—was up-regulated across all 4 comparisons (on average, a 1.60 ± 0.48-fold change in differential gene expression, $p < 0.05$ for all comparisons). The *RELN* gene encodes the protein reelin, which has been shown to influence morphology, membrane permeability, and membrane resistance of vascular endothelial cells as a means of vessel wall integrity regulation.[59] More specifically, reelin increases endothelial cell expression of pro-adhesive VCAM-1, ICAM-1, and E-selectin, resulting in increased monocyte-endothelial activation, inflammation, and adhesion.[60] To date, reelin has not been explored in SCD. However, our data suggests that upregulation of endothelial cell *RELN* expression in response to hypoxic preconditioning may contribute to a pro-adhesive environment. This is notable, as inhibition or reduction of circulating reelin has been proposed a possible approach for the prevention of cardiovascular disease due to its protection against atherosclerosis.[60] Therefore, further studies exploring reelin within the context of SCD are warranted in order to

ascertain if reelin inhibition may also be useful in protection against vaso-occlusion in SCD.

Conclusion

Our novel microfluidic platform fulfills an unmet need in microvascular research. Using sickle RBCs, we leveraged our platform to investigate the likelihood of donor blood samples to occlude on-chip and also to explore hypoxia-induced endothelial gene modulation. Collectively, these results offer a better understanding of the mechanistic changes affecting the endothelium during H/R and also supports the theory that in certain types of hypoxia conditioning may offer a protective effect against vaso-occlusion in SCD.

Conflicts of interest

J. D. Beckman receives research funding from Bayer and Novartis independent from work herein.

Data availability

Supplementary information is available: The SI contains Supplementary Figures and Supplementary Tables. The Tables provide information about blood samples used in this study and additional RNA sequencing information. See DOI: https://doi.org/10.1039/D5LC00211G.

Data supporting this article has been included as a part of the SI.

of Children's Hospitals and Clinics of Minnesota, and Dr. Yvonne Datta of University of Minnesota Medical Center.

References

1 G. J. Kato, F. B. Piel, C. D. Reid, M. H. Gaston, K. Ohene-Frempong and L. Krishnamurti, et al., Sickle cell disease, Nat. Rev. Dis. Primers, 2018, 4, 1–22.

2 P. Sundd, M. T. Gladwin and E. M. Novelli, Pathophysiology of Sickle Cell Disease, 2018, 263–292.

3 J. Weatherall David, The inherited diseases of hemoglobin are an emerging global health burden, Blood, 2010, 115(22), 4331–4336.

4 F. B. Piel, S. I. Hay, S. Gupta, D. J. Weatherall and T. N. Williams, Global Burden of Sickle Cell Anaemia in Children under Five, 2010–2050: Modelling Based on Demographics, Excess Mortality, and Interventions. Osrin D, editor, PLoS Med., 2013, 10(7), e1001484.

5 K. L. Hassell, Population Estimates of Sickle Cell Disease in the U.S, Am. J. Prev. Med., 2010, 38(4), S512–S521.

6 R. P. Hebbel, Ischemia-reperfusion injury in sickle cell anemia: Relationship to acute chest syndrome, endothelial dysfunction, arterial vasculopathy, and inflammatory pain, Hematol./Oncol. Clin. North Am., 2014, 28(2), 181–198.

7 R. P. Hebbel, J. D. Belcher and G. M. Vercellotti, The multifaceted role of ischemia/reperfusion in sickle cell anemia, J. Clin. Invest., 2020, 130(3), 1062–1072.

8 J. D. Belcher, H. Mahaseth, T. E. Welch, A. E. Vilback, K. M. Sonbol and V. S. Kalambur, et al., Critical role of endothelial cell activation in hypoxia-induced vasoocclusion in transgenic sickle mice, Am. J. Physiol., 2005, 288(6), H2715–H2725.

9 J. Ansari and F. N. E. Gavins, Ischemia-Reperfusion Injury in Sickle Cell Disease: From Basics to Therapeutics, Am. J. Pathol., 2019, 189(4), 706–718.

10 T. Kalogeris, C. P. Baines, M. Krenz and R. J. Korthuis, Ischemia/Reperfusion, Compr. Physiol., 2016, 7(1), 113–170.

11 I. Baldea, I. Teacoe, D. E. Olteanu, C. Vaida-Voievod, A. Clichici and A. Sirbu, et al., Effects of different hypoxia degrees on endothelial cell cultures-Time course study, Mech. Ageing Dev., 2018, 172, 45–50.

12 A. Siciliano, G. Malpeli, O. S. Platt, C. Lebouef, A. Janin and A. Scarpa, et al., Abnormal modulation of cell protective systems in response to ischemic/reperfusion injury is important in the development of mouse sickle cell hepatopathy, Haematologica, 2011, 96(1), 24–32.

13 B. Chatel, L. A. Messonnier, C. Vilmen, M. Bernard, V. Pialoux and D. Bendahan, Exacerbated metabolic changes in skeletal muscle of sickle cell mice submitted to an acute ischemia-reperfusion paradigm, Clin. Sci., 2018, 132(19), 2103–2115.

14 J. W. Thompson, K. R. Dave, J. I. Young and M. A. Perez-Pinzon, Ischemic preconditioning alters the epigenetic profile of the brain from ischemic intolerance to ischemic tolerance, Neurotherapeutics, 2013, 10(4), 789–797.

15 M. Azul, E. F. Vital, W. A. Lam, D. K. Wood and J. D. Beckman, Microfluidic methods to advance mechanistic

understanding and translational research in sickle cell disease, *Transl. Res.*, 2022, **246**, 1–14.

16 R. G. Mannino, Y. Qiu and W. A. Lam, Endothelial cell culture in microfluidic devices for investigating microvascular processes, *Biomicrofluidics*, 2018, **12**(4), 042203.

17 C. A. Hesh, Y. Qiu and W. A. Lam, Vascularized microfluidics and the blood-endothelium interface, *Micromachines*, 2020, **11**(1), 18.

18 Y. Sakurai, E. T. Hardy, B. Ahn, R. Tran, M. E. Fay and J. C. Ciciliano, *et al.*, A microengineered vascularized bleeding model that integrates the principal components of hemostasis, *Nat. Commun.*, 2018, **9**(1), 509.

19 D. R. Myers, Y. Sakurai, R. Tran, B. Ahn, E. T. Hardy and R. Mannino, *et al.*, Endothelialized Microfluidics for Studying Microvascular Interactions in Hematologic Diseases, *J. Visualized Exp.*, 2012, **64**, 3958.

20 M. Tsai, A. Kita, J. Leach, R. Rounsevell, J. N. Huang and J. Moake, *et al.*, In vitro modeling of the microvascular occlusion and thrombosis that occur in hematologic diseases using microfluidic technology, *J. Clin. Invest.*, 2012, **122**(1), 408–418.

21 Y. Qiu, B. Ahn, Y. Sakurai, C. E. Hansen, R. Tran and P. N. Mimche, *et al.*, Microvasculature-on-a-chip for the long-term study of endothelial barrier dysfunction and microvascular obstruction in disease, *Nat. Biomed. Eng.*, 2018, **2**, 453–463.

22 M. Kim, Y. Alapan, A. Adhikari, J. A. Little and U. A. Gurkan, Hypoxia-enhanced adhesion of red blood cells in microscale flow, *Microcirculation*, 2017, **24**(5), e12374.

23 C. Caruso, X. Zhang, Y. Sakurai, W. Li, M. E. Fay and M. A. Carden, *et al.*, Stiff Erythrocyte Subpopulations Biomechanically Induce Endothelial Inflammation in Sickle Cell Disease, *Blood*, 2019, **134**(Supplement_1), 3560–3560.

24 N. Naik, D. Hanjaya-Putra, C. A. Haller, M. G. Allen and E. L. Chaikof, Rapid homogeneous endothelialization of high aspect ratio microvascular networks, *Biomed. Microdevices*, 2015, **17**(4), 83.

25 X. Li, S. Xu, P. He and Y. Liu, In vitro recapitulation of functional microvessels for the study of endothelial shear response, nitric oxide and [Ca2+]i, *PLoS One*, 2015, **10**(5), e0126797.

26 Y. Man, R. An, K. Monchamp, Z. Sekyonda, E. Kucukal and C. Federici, *et al.*, OcclusionChip: A functional microcapillary occlusion assay complementary to ektacytometry for detection of small-fraction red blood cells with abnormal deformability, *Front. Physiol.*, 2022, **13**, 954106.

27 Y. Man, E. Kucukal, R. An, Q. D. Watson, J. Bosch and P. A. Zimmerman, *et al.*, Microfluidic assessment of red blood cell mediated microvascular occlusion, *Lab Chip*, 2020, **20**(12), 2086–2099.

28 X. Zhang, T. Chan, J. Carbonella, X. Gong, N. Ahmed and C. Liu, *et al.*, A microfluidic-informatics assay for quantitative physical occlusion measurement in sickle cell disease, *Lab Chip*, 2022, **22**(6), 1126–1136.

29 Y. Qiang, D. Dieujuste, J. Liu, O. Alvarez and E. Du, Rapid electrical impedance detection of sickle cell vaso-occlusion in microfluidic device, *Biomed. Microdevices*, 2023, **25**(3), 23.

30 S. Hansen, D. K. Wood and J. M. Higgins, 5-(Hydroxymethyl) furfural restores low-oxygen rheology of sickle trait blood in vitro, *Br. J. Haematol.*, 2020, **188**(6), 985–993.

31 S. Hansen and D. K. Wood, Simultaneous quantification of blood rheology and oxygen saturation to evaluate affinity-modifying therapies in sickle cell disease, *Lab Chip*, 2022, **22**(21), 4141–4150.

32 J. M. Valdez, Y. H. Datta, J. M. Higgins and D. K. Wood, A microfluidic platform for simultaneous quantification of oxygen-dependent viscosity and shear thinning in sickle cell blood, *APL Bioeng.*, 2019, **3**(4), 046102.

33 H. M. Szafraniec, J. M. Valdez, E. Iffrig, W. A. Lam, J. M. Higgins and P. Pearce, *et al.*, Feature tracking microfluidic analysis reveals differential roles of viscosity and friction in sickle cell blood, *Lab Chip*, 2022, **22**(8), 1565–1575.

34 X. Lu, D. K. Wood and J. M. Higgins, Deoxygenation Reduces Sickle Cell Blood Flow at Arterial Oxygen Tension, *Biophys. J.*, 2016, **110**(12), 2751–2758.

35 Y. Xu, P. Deng, G. Yu, X. Ke, Y. Lin and X. Shu, *et al.*, Thrombogenicity of microfluidic chip surface manipulation: Facile, one-step, none-protein technique for extreme wettability contrast micropatterning, *Sens. Actuators, B*, 2021, **343**, 130085.

36 J. M. Higgins, D. T. Eddington, S. N. Bhatia and L. Mahadevan, Sickle cell vasoocclusion and rescue in a microfluidic device, *Proc. Natl. Acad. Sci. U. S. A.*, 2007, **104**(51), 20496–20500.

37 L. Kim, Y. C. Toh, J. Voldman and H. Yu, A practical guide to microfluidic perfusion culture of adherent mammalian cells, *Lab Chip*, 2007, **7**(6), 681–694.

38 E. Ortiz-Prado, J. F. Dunn, J. Vasconez, D. Castillo and G. Viscor, Partial pressure of oxygen in the human body: a general review, *Am. J. Blood Res.*, 2019, **9**(1), 1–14.

39 G. Malatesha, N. K. Singh, A. Bharija, B. Rehani and A. Goel, Comparison of arterial and venous pH, bicarbonate, PCO2 and PO2 in initial emergency department assessment, *Emerg. Med. J.*, 2007, **24**(8), 569–571.

40 C. Tellier, D. Desmet, L. Petit, L. Finet, C. Graux and M. Raes, *et al.*, Cycling hypoxia induces a specific amplified inflammatory phenotype in endothelial cells and enhances tumor-promoting inflammation in vivo, *Neoplasia*, 2015, **17**(1), 66–78.

41 D. K. Kaul, E. Finnegan and G. A. Barabino, Sickle red cell-endothelium interactions, *Microcirculation*, 2009, **16**(1), 97–111.

42 M. J. Telen, P. Malik and G. M. Vercellotti, Therapeutic strategies for sickle cell disease: towards a multi-agent approach, *Nat. Rev. Drug Discovery*, 2019, **18**(2), 139–158.

43 R. Steward, D. Tambe, C. C. Hardin, R. Krishnan and J. J. Fredberg, Fluid shear, intercellular stress, and endothelial cell alignment, *Am. J. Physiol.*, 2015, **308**(8), C657–C664.

44 C. Cerutti and A. J. Ridley, Endothelial cell-cell adhesion and signaling, *Exp. Cell Res.*, 2017, **358**(1), 31–38.

45 N. Prasain and T. Stevens, The actin cytoskeleton in endothelial cell phenotypes, *Microvasc. Res.*, 2009, **77**(1), 53–63.

46 W. D. Ehringer, S. Yamany, K. Steier, A. Farag, F. J. Roisen and A. Dozier, *et al.*, Quantitative Image Analysis of F-Actin in Endothelial Cells, *Microcirculation*, 1999, **6**(4), 291–303.

47 D. Tousoulis, A. M. Kampoli, C. Tentolouris, N. Papageorgiou and C. Stefanadis, The role of nitric oxide on endothelial function, *Curr. Vasc. Pharmacol.*, 2012, **10**(1), 4–18.

48 Y. May, R. An, K. Monchamp, Z. Sekyonda, E. Kucukal, C. Federici, W. J. Wulftange, U. Goreke, A. Bode, V. A. Sheehan and U. A. Gurkan, OcclusionChip: A Functional Microcapillary Occlusion Assay Complementary to Ektacytometry for Assessing Red Cell Health in Sickle Cell Disease, *Front. Physiol.*, 2022, **13**, 954106.

49 M. E. Fay, O. Oshinowo, E. Iffrig, K. S. Fibben, C. Caruso and S. Hansen, *et al.*, iCLOTS: open-source, artificial intelligence-enabled software for analyses of blood cells in microfluidic and microscopy-based assays, *Nat. Commun.*, 2023, **14**, 5022.

50 A. Habara and M. H. Steinberg, Minireview: Genetic basis of heterogeneity and severity in sickle cell disease, *Exp. Biol. Med.*, 2016, **241**(7), 689–696.

51 F. B. Piel, M. H. Steinberg and D. C. Rees, Sickle Cell Disease, *N. Engl. J. Med.*, 2017, 1561–1573.

52 G. Ceglie, M. Di Mauro, I. Tarissi De Jacobis, F. de Gennaro, M. Quaranta and C. Baronci, *et al.*, Gender-Related Differences in Sickle Cell Disease in a Pediatric Cohort: A Single-Center Retrospective Study, *Front. Mol. Biosci.*, 2019, **6**, 140.

53 O. S. Platt, D. J. Brambilla, W. F. Rosse, P. F. Milner, O. Castro and M. H. Steinberg, *et al.*, Mortality in sickle cell disease. Life expectancy and risk factors for early death, *N. Engl. J. Med.*, 1994, **330**(23), 1639–1644.

54 D. Zhang, C. Xu, D. Manwani and P. S. Frenette, Neutrophils, platelets, and inflammatory pathways at the nexus of sickle cell disease pathophysiology, *Blood*, 2016, **127**(7), 801–809.

55 C. Liu, Z. Li and H. Xi, Bioinformatics analysis and in vivo validation of ferroptosis-related genes in ischemic stroke, *Front. Pharmacol.*, 2022, **13**, 940260.

56 M. O. S. Carvalho, A. L. C. S. Souza, M. B. Carvalho, A. P. A. S. Pacheco, L. C. Rocha and d. N. VML, *et al.*, Evaluation of Alpha-1 Antitrypsin Levels and SERPINA1 Gene Polymorphisms in Sickle Cell Disease, *Front. Immunol.*, 2017, **8**, 1491.

57 J. Riis, B. G. Nordestgaard and S. Afzal, α1-Antitrypsin Z allele and risk of venous thromboembolism in the general population, *J. Thromb. Haemostasis*, 2022, **20**(1), 115–125.

58 D. S. DeLuca, E. Poluzioroviene, V. Taminskiene, S. Wrenger, A. Utkus and A. Valiulis, *et al.*, SERPINA1 gene polymorphisms in a population-based ALSPAC cohort, *Pediatr. Pulmonol.*, 2019, **54**(9), 1474–1478.

59 E. Scott, T. J. Dougherty, G. Gorski and C. J. Hatcher, Reelin Signaling in Vascular Endothelial Cell Biology, *FASEB J.*, 2019, **33**, 83.4.

60 Y. Ding, L. Huang, X. Xian, I. S. Yuhanna, C. R. Wasser and M. Frotscher, *et al.*, Loss of Reelin protects against atherosclerosis by reducing leukocyte-endothelial cell adhesion and lesion macrophage accumulation, *Sci. Signaling*, 2016, **9**(419), ra29.